

Hamiltonian design in readout from room-temperature Raman atomic memory

Michał Dąbrowski, Radosław Chrapkiewicz,* and Wojciech
Wasilewski

Institute of Experimental Physics, University of Warsaw, Pasteura 5, 02-093 Warsaw, Poland

[*radekch@fuw.edu.pl](mailto:radekch@fuw.edu.pl)

Abstract: We present an experimental demonstration of the Hamiltonian manipulation in light-atom interface in Raman-type warm rubidium-87 vapor atomic memory. By adjusting the detuning of the driving beam we varied the relative contributions of the Stokes and anti-Stokes scattering to the process of four-wave mixing which reads out a spatially multimode state of atomic memory. We measured the temporal evolution of the readout fields and the spatial intensity correlations between write-in and readout as a function of detuning with the use of an intensified camera. The correlation maps enabled us to resolve between the anti-Stokes and the Stokes scattering and to quantify their contributions. Our experimental results agree quantitatively with a simple, plane-wave theoretical model we provide. They allow for a simple interpretation of the coaction of the anti-Stokes and the Stokes scattering at the readout stage. The Stokes contribution yields additional, adjustable gain at the readout stage, albeit with inevitable extra noise. Here we provide a simple and useful framework to trace it and the results can be utilized in the existing atomic memories setups. Furthermore, the shown Hamiltonian manipulation offers a broad range of atom-light interfaces readily applicable in current and future quantum protocols with atomic ensembles.

© 2021 Optical Society of America

OCIS codes: (270.5585) Quantum information and processing; (020.0020) Atomic and molecular physics; (290.5910) Scattering, stimulated Raman; (190.4380) Nonlinear optics, four-wave mixing.

References and links

1. A. I. Lvovsky, B. C. Sanders, and W. Tittel, “Optical quantum memory,” *Nature Photon.* **3**, 706–714 (2009).
2. L. M. Duan, M. D. Lukin, J. I. Cirac, and P. Zoller, “Long-distance quantum communication with atomic ensembles and linear optics,” *Nature* **414**, 413–418 (2001).
3. H. J. Kimble, “The quantum internet,” *Nature* **453**, 1023–30 (2008).
4. J. Nunn, N. Langford, W. Kolthammer, T. Champion, M. Sprague, P. Michelberger, X. M. Jin, D. England, and I. Walmsley, “Enhancing Multiphoton Rates with Quantum Memories,” *Phys. Rev. Lett.* **110**, 133601 (2013).
5. P. Kok, K. Nemoto, T. C. Ralph, J. P. Dowling, and G. J. Milburn, “Linear optical quantum computing with photonic qubits,” *Rev. Mod. Phys.* **79**, 135–174 (2007).
6. A. Chiuri, C. Greganti, L. Mazzola, M. Paternostro, and P. Mataloni, “Linear optics simulation of quantum non-Markovian dynamics,” *Sci. Rep.* **2**, 968 (2012).
7. A. Aspuru-Guzik and P. Walther, “Photonic quantum simulators,” *Nature Phys.* **8**, 285–291 (2012).
8. P. Neumann, R. Kolesov, B. Naydenov, J. Beck, F. Rempp, M. Steiner, V. Jacques, G. Balasubramanian, M. L. Markham, D. J. Twitchen, S. Pezzagna, J. Meijer, J. Twamley, F. Jelezko, and J. Wrachtrup, “Quantum register based on coupled electron spins in a room-temperature solid,” *Nature Phys.* **6**, 249–253 (2010).

9. P. C. Maurer, G. Kucsko, C. Latta, L. Jiang, N. Y. Yao, S. D. Bennett, F. Pastawski, D. Hunger, N. Chisholm, M. Markham, D. J. Twitchen, J. I. Cirac, and M. D. Lukin, "Room-temperature quantum bit memory exceeding one second," *Science* **336**, 1283–1286 (2012).
10. M. Hosseini, B. M. Sparkes, G. Campbell, P. K. Lam, and B. C. Buchler, "High efficiency coherent optical memory with warm rubidium vapour," *Nature Commun.* **2**, 174 (2011).
11. D. B. Higginbottom, B. M. Sparkes, M. Rancic, O. Pinel, M. Hosseini, P. K. Lam, and B. C. Buchler, "Spatial-mode storage in a gradient-echo memory," *Phys. Rev. A* **86**, 023801 (2012).
12. K. F. Reim, J. Nunn, V. O. Lorenz, B. J. Sussman, K. C. Lee, N. K. Langford, D. Jaksch, and I. A. Walmsley, "Towards high-speed optical quantum memories," *Nature Photon.* **4**, 218–221 (2010).
13. K. Reim, P. Michelberger, K. Lee, J. Nunn, N. Langford, and I. Walmsley, "Single-Photon-Level Quantum Memory at Room Temperature," *Phys. Rev. Lett.* **107**, 053603 (2011).
14. S. E. Harris, "Electromagnetically Induced Transparency," *Physics Today* **50**(7), 36–42 (1997).
15. M. Fleischhauer and M. D. Lukin, "Dark-state polaritons in electromagnetically induced transparency," *Phys. Rev. Lett.* **84**, 5094–5097 (2000).
16. M. D. Lukin and A. Imamoglu, "Controlling photons using electromagnetically induced transparency," *Nature* **413**, 273–276 (2001).
17. M. Fleischhauer, A. Imamoglu, and J. Marangos, "Electromagnetically induced transparency: Optics in coherent media," *Rev. Mod. Phys.* **77**, 633–673 (2005).
18. M. Bashkansky, F. K. Fatemi, and I. Vurgaftman, "Quantum memory in warm rubidium vapor with buffer gas," *Opt. Lett.* **37**, 142–144 (2012).
19. R. Chrapkiewicz and W. Wasilewski, "Generation and delayed retrieval of spatially multimode Raman scattering in warm rubidium vapours," *Opt. Express* **20**, 29540–29551 (2012).
20. R. Chrapkiewicz, W. Wasilewski, and C. Radzewicz, "How to measure diffusional decoherence in multimode rubidium vapor memories?," *Opt. Commun.* **317**, 1–6 (2014).
21. K. Jensen, W. Wasilewski, H. Krauter, T. Fernholz, B. M. Nielsen, M. Owari, M. B. Plenio, a. Serafini, M. M. Wolf, and E. S. Polzik, "Quantum memory for entangled continuous-variable states," *Nature Phys.* **7**, 13–16 (2010).
22. P. K. Vudyasethu, R. M. Camacho, and J. C. Howell, "Storage and Retrieval of Multimode Transverse Images in Hot Atomic Rubidium Vapor," *Phys. Rev. Lett.* **100**, 123903 (2008).
23. O. Firstenberg, M. Shuker, A. Ron, and N. Davidson, "Colloquium: Coherent diffusion of polaritons in atomic media," *Rev. Mod. Phys.* **85**, 941–960 (2013).
24. S. de Echaniz, M. Koschorreck, M. Napolitano, M. Kubasik, and M. Mitchell, "Hamiltonian design in atom-light interactions with rubidium ensembles: A quantum-information toolbox," *Phys. Rev. A* **77**, 032316 (2008).
25. P. S. Michelberger, T. F. M. Champion, M. R. Sprague, K. T. Kaczmarek, M. Barbieri, X. M. Jin, D. G. England, W. S. Kolthammer, D. J. Saunders, J. Nunn, and I. A. Walmsley, "Interfacing GHz-bandwidth heralded single photons with a room-temperature Raman quantum memory," arXiv:1405.1470.
26. M. G. Raymer, "Quantum state entanglement and readout of collective atomic-ensemble modes and optical wave packets by stimulated Raman scattering," *J. Mod. Opt.* **51**, 1739–1759 (2004).
27. W. Wasilewski and M. Raymer, "Pairwise entanglement and readout of atomic-ensemble and optical wave-packet modes in traveling-wave Raman interactions," *Phys. Rev. A* **73**, 063816 (2006).
28. A. Gorshkov, A. André, M. Lukin, and A. S. Sørensen, "Photon storage in Λ -type optically dense atomic media. II. Free-space model," *Phys. Rev. A* **76**, 033805 (2007).
29. E. Zeuthen, A. Grodecka-Grad, and A. S. Sørensen, "Three-dimensional theory of quantum memories based on Λ -type atomic ensembles," *Phys. Rev. A* **84**, 043838 (2011).
30. W. Wasilewski, T. Fernholz, K. Jensen, L. S. Madsen, H. Krauter, C. Muschik, and E. S. Polzik, "Generation of two-mode squeezed and entangled light in a single temporal and spatial mode," *Opt. Express* **17**, 14444–14457 (2009).
31. C. Vitelli, N. Spagnolo, L. Toffoli, F. Sciarrino, and F. De Martini, "Enhanced Resolution of Lossy Interferometry by Coherent Amplification of Single Photons," *Phys. Rev. Lett.* **105**, 113602 (2010).
32. S. Fossier, E. Diamanti, T. Debuisschert, R. Tualle-Brouri, and P. Grangier, "Improvement of continuous-variable quantum key distribution systems by using optical preamplifiers," *J. Phys. B* **42**, 114014 (2009).
33. J. Kolodyński, J. Chwedeńczuk, and W. Wasilewski, "Eigenmode description of Raman scattering in atomic vapors in the presence of decoherence," *Phys. Rev. A* **86**, 013818 (2012).
34. H. Krauter, D. Salart, C. A. Muschik, J. M. Petersen, H. Shen, T. Fernholz, and E. S. Polzik, "Deterministic quantum teleportation between distant atomic objects," *Nature Phys.* **9**, 400–404 (2013).
35. M. G. Raymer and J. Mostowski, "Stimulated Raman scattering: Unified treatment of spontaneous initiation and spatial propagation," *Phys. Rev. A* **24**, 1980–1993 (1981).
36. A. Gorshkov, A. André, M. Lukin, and A. S. Sørensen, "Photon storage in Λ -type optically dense atomic media. I. Cavity model," *Phys. Rev. A* **76**, 033804 (2007).
37. V. Boyer, A. M. Marino, R. C. Pooser, and P. D. Lett, "Entangled images from four-wave mixing," *Science* **321**, 544–547 (2008).
38. C. H. van der Wal, M. D. Eisaman, A. Andre, R. L. Walsworth, D. F. Phillips, A. S. Zibrov, and M. D. Lukin,

- “Atomic Memory for Correlated Photon States,” *Science* **301**, 196–200 (2003).
39. D. J. McCarron, I. G. Hughes, P. Tierney, and S. L. Cornish, “A heated vapor cell unit for dichroic atomic vapor laser lock in atomic rubidium,” *Rev. Sci. Instrum.* **78**, 093106 (2007).
 40. R. Chrapkiewicz, W. Wasilewski, and K. Banaszek, “High-fidelity spatially resolved multiphoton counting for quantum imaging applications,” *Opt. Lett.* **39**, 5090-5093 (2014).
 41. R. Chrapkiewicz, “Photon counts statistics of squeezed and multimode thermal states of light on multiplexed on–off detectors,” *J. Opt. Soc. Am. B* **31**, B8-B13 (2014).
 42. P. A. Moreau, F. Devaux, and E. Lantz, “The Einstein-Podolsky-Rosen paradox in twin images,” arXiv:1404.3028.
 43. M. Shuker, O. Firstenberg, R. Pugatch, A. Ron, and N. Davidson, “Storing Images in Warm Atomic Vapor,” *Phys. Rev. Lett.* **100**, 223601 (2008).
 44. I. Vurgaftman and M. Bashkansky, “Suppressing four-wave mixing in warm-atomic-vapor quantum memory,” *Phys. Rev. A* **87**, 063836 (2013).
-

1. Introduction

On-demand retrieval of pre-stored photons can be accomplished using quantum memories [1]. This is an indispensable technique for long distance quantum communication networks [2, 3] and for the enhanced generation of multi-photon states [4]. Such states find applications in a linear quantum computing scheme [5] or quantum simulators using linear optics [6, 7].

Implementations of quantum memories in room-temperature setups are among the most auspicious in terms of possible future applications due to their robustness. Until now room-temperature quantum memories have been realized in solid state systems [8, 9] and in warm atomic ensembles [1] such as gradient echo memory [10, 11], Raman memory [12, 13] or EIT memory [14–17].

In this paper we focus on Raman-type atomic memory implemented in warm rubidium-87 vapors [18–20]. In such memory photons are stored in atomic collective excitations called spin-waves. They are interfaced to photons via off-resonant Raman transitions. Storage times up to 30 ms in a single spin-wave mode was demonstrated [21]. Multimode storage, both temporal [10] and spatial [11, 19], is also feasible. With the use of multiple transverse spin-wave modes images can be stored and retrieved [22, 23]. The storage time of the multimode memory is limited by diffusional decoherence and thus can be prolonged by increasing the beam size [20, 23] at the expense of laser intensity.

Here we demonstrate experimentally the theoretical concept of “Hamiltonian design” proposed in [24]. We implement the Hamiltonian design at the readout from Raman atomic memory. Ideal readout from Raman atomic memory relies on a pure anti-Stokes scattering process which maps the spin-wave state onto photons state. In real systems additional Stokes scattering at the readout is virtually inevitable and it is a source of extra noise [13, 25]. By modifying the interaction Hamiltonian we are able to control the relative contributions of anti-Stokes and Stokes scattering processes. In the particular setting of our experiment this enables parametric amplification of the readout, albeit with extra noise.

In this paper we use simple theoretical model describing the coaction between anti-Stokes and Stokes scattering in readout. Previous approaches to describe theoretically the readout of spin-wave excitations in Raman scattering were focused only on pure anti-Stokes process. Theoretical descriptions of readout from Raman-type memory have already been given for a number of cases, including spatio-temporal evolution with losses [26], temporal eigen-modes [27], optimized retrieval [28], and spatial modes [29]. However, in those papers emphasis was put on the pure anti-Stokes scattering. In the present paper we use the extended description of the readout process [30], taking into account the four-wave mixing that includes the Stokes scattering.

In the experiment we detect scattered light with spatial resolution and temporal gating. This enables directly relating the experimental results to the theoretical predictions for temporal

evolution of scattered light. Stokes and anti-Stokes light contributions can be distinguished through intensity correlation measurements and quantified via careful post-processing.

We provide evidence for a possibility of engineering a wide range of atom-light interfaces which can be described theoretically as simultaneous readout and parametric amplification. This may enable enriching purely optical quantum metrology [31] or communication [32] schemes with quantum storage capabilities.

This paper is organized as follows: In Sec. 2 we introduce a single-mode, theoretical model of temporal evolution of Stokes and anti-Stokes in readout, Sec. 3 describe experimental details, in Sec. 4 we present the phenomenological model utilized for data analysis and the results; finally Sec. 5 concludes the paper.

2. Theory

We begin by synthesizing a simple, plane-wave theoretical model of the readout by four-wave mixing from a Raman memory to qualitatively support our experimental results. The spin-wave excitation in the atomic medium can be created by different means. Light can be absorbed in a two-photon Raman transition to store previously prepared state of light [13, 25]. In our experiment we induced spontaneous Stokes scattering using write pulse with a wave vector \mathbf{k}_W to populate the spin-waves, i.e. collective atomic excitations from the levels $|0\rangle$ to $|1\rangle$ as in Fig. 1(a). Both approaches results in the spin-wave excitation, however the latter which we use

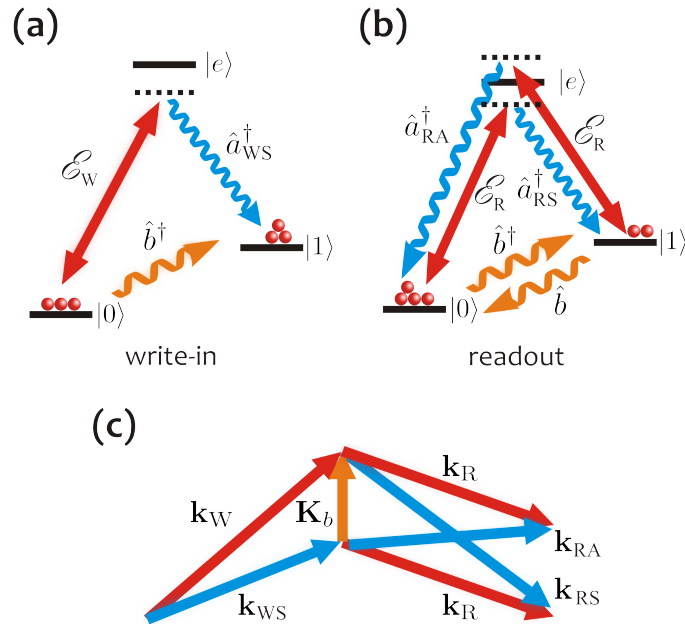


Fig. 1. Atomic levels and phase matching in Λ -scheme Raman scattering induced by classical laser field \mathcal{E}_W and \mathcal{E}_R . (a) In the spontaneous write-in process Stokes photons (\hat{a}_{WS}^\dagger - mode) and spin-wave excitation (\hat{b}^\dagger - mode) are created pairwise. (b) Four-wave mixing in readout consists in simultaneous anti-Stokes and Stokes scattering into modes \hat{a}_{RA}^\dagger and \hat{a}_{RS}^\dagger . (c) Phase matching condition or momentum conservation dictates the wave vectors of single photons coupled to a spin-wave excitation with a certain wave vector \mathbf{K}_b . Write beam with \mathbf{k}_W wave vector is scattered as Stokes photon with \mathbf{k}_{WS} wave vector, while read beam with \mathbf{k}_R wave vector either scatters Stokes or couples anti-Stokes of the respective wave vectors \mathbf{k}_{RS} , \mathbf{k}_{RA} .

does not require special efforts to match the photons from the external source to the memory bandwidth. Ideally, the number of created spin-wave excitations n_b with a certain wave vector \mathbf{K}_b equals the number of scattered Stokes photons with wave vector $\mathbf{k}_{\text{WS}} = \mathbf{k}_{\text{W}} - \mathbf{K}_b$. We were able to estimate those numbers in each single iteration of the experiment.

Here we focused on the retrieval stage at which the spin-wave excitations are converted to photons in four-wave mixing induced by the read laser pulse depicted in Fig.1(b). The read laser is assumed to be plane-wave with a wave vector \mathbf{k}_R . Spin-wave with a certain wave vector \mathbf{K}_b are coupled to anti-Stokes and Stokes fields with wave vectors $\mathbf{k}_{\text{RA}} = \mathbf{k}_R + \mathbf{K}_b$ and $\mathbf{k}_{\text{RS}} = \mathbf{k}_R - \mathbf{K}_b$ respectively. In the experiment those weak light fields illuminated distinct pixels of the camera which was located in the far field. They were also shifted with respect to the initial Stokes photons with the wave vector $\mathbf{k}_{\text{WS}} = \mathbf{k}_{\text{W}} - \mathbf{K}_b$ due to different direction of the write beam \mathbf{k}_{W} . We summarize the phase matching condition relating the wave vectors in Fig. 1(c).

To describe the interaction at the readout stage we use bosonic operators of the weak field light modes \hat{a}_{RA} and \hat{a}_{RS} . The spin-wave can be described with the Holstein-Primakhoff approximation by a bosonic annihilation operator \hat{b} which removes one excitation from spin-wave with the wave vector \mathbf{K}_b [33]. The Hamiltonian describing both the Stokes and anti-Stokes scattering at the readout stage can be obtained by eliminating the excited level adiabatically [30, 34]:

$$\hat{H}_R = i\hbar\chi\hat{a}_{\text{RA}}^\dagger\hat{b} + i\hbar\xi\hat{a}_{\text{RS}}^\dagger\hat{b}^\dagger + H.c. \quad (1)$$

where χ and ξ are the coupling coefficients for anti-Stokes and Stokes Raman transitions [35]. The coupling coefficients squared χ^2 or ξ^2 can be calculated [36] as $\Gamma d\Omega_p^2/\Delta^2$ where d is optical depth at resonance, Ω_p is the pump Raman frequency and Δ is the detuning of the pump from transition from level 1 or 0 to excited state for anti-Stokes coupling χ^2 or ξ^2 respectively. Such a Hamiltonian (Eq. (1)) has been used in several papers describing experiments on room-temperature atomic vapors, i.e. teleportation between distant atomic objects [34].

The above Hamiltonian leads to coupled Maxwell-Bloch equations, which can be integrated as e.g. in [30, 33]. This yields input-output relations linking the operators of the incoming light fields and the initial spin-wave state to the outgoing fields and the final spin-wave state.

We used the input-output relations to compute the quantities observed in the experiments, that is the mean number of scattered photons as a function of time in anti-Stokes $\langle\hat{a}_{\text{RA}}^\dagger(t)\hat{a}_{\text{RA}}(t)\rangle$ and Stokes fields $\langle\hat{a}_{\text{RS}}^\dagger(t)\hat{a}_{\text{RS}}(t)\rangle$ respectively. With the assumption that the incoming light fields are in a vacuum state and the mean number of initial spin-wave excitations equals $n_b = \langle\hat{b}^\dagger(0)\hat{b}(0)\rangle$, the result is:

$$\langle\hat{a}_{\text{RA}}^\dagger(t)\hat{a}_{\text{RA}}(t)\rangle = \underbrace{\chi^2 e^{t(\xi^2 - \chi^2)}}_{G_{\text{RA}}(t)} n_b + \underbrace{\frac{\chi^2 \xi^2}{\xi^2 - \chi^2} (e^{t(\xi^2 - \chi^2)} - 1)}_{S_{\text{RA}}(t)}, \quad (2)$$

$$\langle\hat{a}_{\text{RS}}^\dagger(t)\hat{a}_{\text{RS}}(t)\rangle = \underbrace{\xi^2 e^{t(\xi^2 - \chi^2)}}_{G_{\text{RS}}(t)} n_b + \underbrace{\frac{\xi^2}{\xi^2 - \chi^2} (\xi^2 e^{t(\xi^2 - \chi^2)} - \chi^2)}_{S_{\text{RS}}(t)}, \quad (3)$$

The underbraced terms $G_{\text{RA}}(t)$ and $G_{\text{RS}}(t)$ represent the readout gains, that is the number of scattered photons per each input spin-wave excitation. In turn, the terms $S_{\text{RA}}(t)$ and $S_{\text{RS}}(t)$ represent the spontaneous scattering into anti-Stokes and Stokes quantum fields, which is independent of the initial state of quantum fields. Just as expected, they appear only in the presence of Stokes scattering $\xi \neq 0$. Note that both coupling coefficients χ and ξ appear in both formulas (2) and (3), confirming that anti-Stokes and Stokes scattering cannot be treated separately and should be viewed together as a full four-wave mixing process.

Note that the above results were derived neglecting all decoherence. In the experiment, the most important sources of decoherence are diffusion of atoms and spontaneous emission from

the excited state in random direction. Both can be neglected provided the optical depth is large and the duration of the interaction short.

Let us proceed to examining the evolution of scattered anti-Stokes and Stokes light in a few typical cases.

For $\xi \simeq 0$ there is virtually no Stokes scattering while the anti-Stokes scattering appears instantaneously and decays exponentially as depicted in Fig. 2(a). There is virtually no spontaneous noise $S_{RA} \simeq 0$ and the time integrated gain reaches unity $\bar{G}_{RA} = \int G_{RA} dt = 1$. In the ideally case of $\xi = 0$ this leads to the readout Hamiltonian of form $\hat{H}_R \sim \hat{a}_{RA}^\dagger \hat{b} + H.c.$ which represent purely anti-Stokes scattering process.

In real systems Stokes interaction is typically unavoidable. The case where $\chi > \xi > 0$ is depicted in Fig. 2(b). Here the readout appears in both the anti-Stokes and Stokes fields with comparable intensity and decays over time. Time-integrated gain may reach over unity $\bar{G}_i = \int G_i dt > 1$, yet with spontaneous noise that slowly builds up $S_i > 0$, for $i = RA, RS$. This is the setting utilized in [37].

A situation where Stokes interaction dominates, $\xi > \chi$, is depicted in Fig. 2(c). In this case readout goes predominantly to Stokes field with exponentially increasing gain. Yet, the noise intensity virtually equals the gain $G_i \simeq S_i$ for both fields. In the limit of $\xi \gg \chi$ we can put $\chi = 0$ which leads to the readout Hamiltonian $\hat{H}_R \sim \hat{a}_{RS}^\dagger \hat{b}^\dagger + H.c.$ consists only the contribution of Stokes scattering process.

It is instructive to integrate gains $G_{RA}(t)$ and $G_{RS}(t)$, and noises $S_{RA}(t)$ and $S_{RS}(t)$ over the time of interaction and inspect them as functions of coupling coefficients. Coupling coefficients χ and ξ are inversely proportional to the detuning of the read laser from the excited level

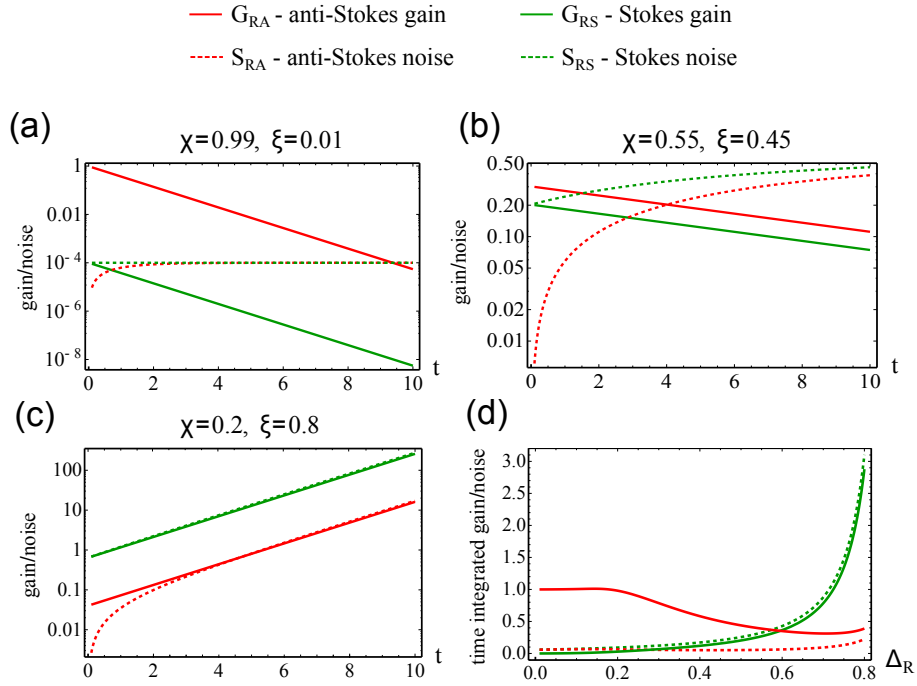


Fig. 2. (a) to (c) - temporal evolution of gains G_i and spontaneous noises S_i building up the light fields. Data plotted for different values of coupling coefficients χ and ξ correspond to detuning parameters $\Delta_R = 0.3, 0.6$ and 0.8 . (d) Integrated readout gains \bar{G}_i and spontaneous noises \bar{S}_i versus detuning Δ_R .

Δ_R [33, 35]. One coupling coefficient can be increased at the expense of the other by tuning the frequency of the read laser when it is in between the $|0\rangle \leftrightarrow |e\rangle$ and $|1\rangle \leftrightarrow |e\rangle$ resonances as in Fig. 1(b).

In Fig. 2 (d) we plot the time integrated gains $\bar{G}_i = \int G_i dt$ and noises $\bar{S}_i = \int S_i dt$ as a function of the detuning Δ_R from $|0\rangle \leftrightarrow |e\rangle$ transition in the units of ground state splitting. We assumed $\chi \propto 1/\Delta_R$ and $\xi \propto 1/(1 - \Delta_R)$. Different characters of anti-Stokes and Stokes interaction causes asymmetry of the plot in Fig. 2 (d). The integrated readout gain in the anti-Stokes domination regime $\chi \gg \xi$ remains equal to unity $\bar{G}_{RA} = 1$ and the noise is suppressed $\bar{S}_{RA} \ll 1$. These are the conditions for perfect unamplified readout.

On the contrary, in the Stokes domination regime $\chi \ll \xi$ the integrated gain \bar{G}_{RS} varies almost exponentially with the Stokes coupling ξ entailing elevated noise \bar{S}_{RS} . In this domain four-wave mixing enhances the anti-Stokes emission and \bar{G}_{RA} rises although the relative contribution $\bar{G}_{RA}/\bar{G}_{RS}$ diminishes. Note that this is the regime we use to populate the spin-waves by inducing spontaneous Stokes scattering with write pulse.

Finally, let us consider a single realization of the four-wave mixing process. Assume that the number of initial spin-wave excitations n_b has been measured by counting the Stokes photons n_{WS} scattered during prior write-in, ideally $n_{WS} = n_b$. In this particular iteration the number of photons in the anti-Stokes and the Stokes field equals

$$n_i = \bar{G}_i n_b + \check{S}_i, \quad i = RS, RA \quad (4)$$

where \check{S}_i is the noise treated here as an independent random variable. \check{S}_i is the time integrated spontaneous scattering and its mean is calculated based on Eqs. (2), (3) $\langle \check{S}_i \rangle = \bar{S}_i$. Later on we refer to the correlation of the number of anti-Stokes n_{RA} or Stokes photons n_{RS} with the initial spin-wave excitation n_b . The above formula links the correlated part to the integrated readout gain \bar{G}_i and the uncorrelated noise to the integrated spontaneous contribution \bar{S}_i .

3. Experiment

We implemented Raman-type atomic memory in rubidium-87 vapors. We applied spontaneous write-in process into memory similarly as in previous works [18, 38]. The spontaneous write-in process had been proven to efficiently create the spin-wave excitations, thus we could focus on the retrieval characteristics. Here we extended the setup and measurements schemes applied and explained in detail in our previous papers [19, 20].

We used a 10 cm glass cell containing pure ^{87}Rb isotope with krypton as a buffer gas under pressure of 1 torr. The cell was heated by bifilar windings to 90°C equivalent to the optical

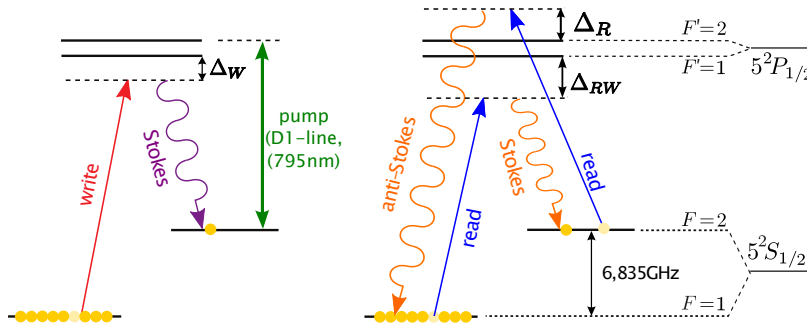


Fig. 3. Configuration schemes of ^{87}Rb hyperfine energy levels at D1 line (795nm) using write-in and readout respectively. Laser beams and scattered light detunings in both processes are also depicted.

density of 135. The cell was magnetically shielded to avoid decoherence produced by stray magnetic field and the main source of decoherence was due to diffusion [20].

We used three external cavity diode lasers: pump, write and read laser, operating at D1 line of ^{87}Rb (795 nm). The frequencies of all laser beams and the scattered light are sketched against the ^{87}Rb level scheme in Fig. 3. The pump laser was resonant to $F=2 \rightarrow F'=2$ transition, while the write and read laser were detuned to the red from transition $F=1 \rightarrow F'=1'$. The detuning of the write laser was $\Delta_W = 1.77$ GHz and it was kept constant throughout all measurements while the detuning of the read laser Δ_R varied. The pump and write lasers were frequency locked using the DAVLL setup [39]. The exact values of the write and read lasers detunings were set repeatedly and measured precisely using Doppler-free saturated absorption spectroscopy inside an auxiliary rubidium cell and their reference beat-note signal was measured on a fast photodiode. Inside the cell write, read and pump lasers had the power of 6.8 mW, 4.5 mW and 75 mW respectively. During the experimental sequence the lasers power fluctuated at a level of 5% and the frequencies were changing by no more than 50MHz.

The simplified schematic of the setup is shown in Fig. 4(a). All of the three horizontally polarized beams overlapped inside the cell where their diameters were 6 mm for the pump beam and 4 mm for both write and read beams. The write and read beams were tilted at the angle $\theta = 2$ mrad. Acousto-optic modulators were used to shape rectangular pulses with rising time of $1 \mu\text{s}$ from laser beams. The pulse sequence applied in the experiment is depicted in Fig. 4(b). The sequence was initiated by optical pumping of rubidium atoms into the ground state of ^{87}Rb $S^{1/2}$ $F=1$. The $700 \mu\text{s}$ long rectangular pulse of 75 mW power yielded a pumping efficiency of 98%. Then we applied a $10 \mu\text{s}$ long rectangular write pulse to create spin-wave excitations between $F=1$ and $F=2$ levels together with the Stokes scattering. The rectangular read pulse started right after the end of the write pulse and its duration was set to $40 \mu\text{s}$. The read pulse generated both anti-Stokes and Stokes scattering. The total time duration of write and read pulse corresponds to the average atomic displacement of c.a. 0.5 mm due to diffusion [20] which was small enough to keep the atoms in the range of the pump beam size.

We separated the horizontally polarized laser beams from the vertically polarized scattered

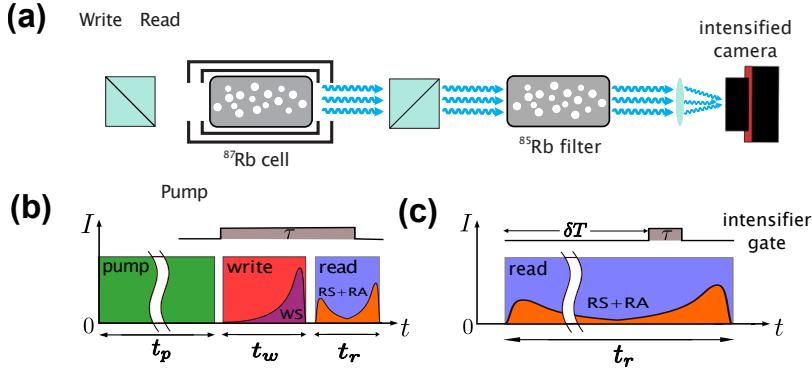


Fig. 4. (a) Experimental setup: write and read laser beams propagate forward to the intensified camera and the pump beam propagates backward. ^{87}Rb - atomic memory cell, ^{85}Rb - absorption filter, blue arrows correspond to scattered light. (b) Pulse sequence with long intensifier gate covers the whole write and a part of the read pulse (both rectangular). Exponential shapes in front of write and read pulses are typical time-resolved intensities of the scattered light observed on the intensified camera, WS and RS stand for Stokes while RA for anti-Stokes scattering respectively. (c) Scheme of the measurement of the temporal evolution of the readout light using short gate duration $\tau = 250$ ns.

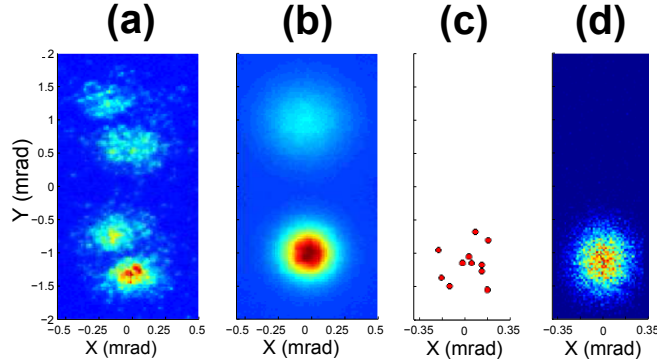


Fig. 5. Representative images of the retrieved field, write-in and read-out in upper and lower parts respectively. (a) Intensity map in a single shot obtained using a long gate in the linear regime of camera operation and (b) the average over 10^4 frames. (c) Photon positions in a single shot [40] obtained using a short gate positioned in the readout stage and (d) the total number of photons per sCMOS pixel summed over 2000 frames.

fields by polarization and spectral filtering, which yielded the total attenuation factor for laser beams that exceeded 10^9 . For spectral filtering we applied a ^{85}Rb absorption filter at 130°C placed in magnetic field which increase the absorption by broadening and shifting the ^{85}Rb spectral lines. The attenuation of laser beams inside the 30 cm length absorption filter was at least 10^4 . We also measured the transmission of the filter at frequencies corresponding to the scattered light generated at write-in and readout stages. They were found to be 12% for Stokes scattering in write-in and 76% for all applied frequencies of anti-Stokes and Stokes in readout.

In our system we generated and retrieved spatially multimode light as described in detail in [19, 33]. This light was detected in the far field by a gated image intensifier coupled to sCMOS camera [40]. We used the intensified camera in two different operational schemes. In the first scheme we applied a long gate pulse which covered both the write and the read pulse as in Fig. 4(b). We set the gain of the intensifier to a low value. Then the response of the camera system was proportional to the intensity of scattered light. We calibrated the excess noise contributed by the image intensifier and made sure that it was insignificant as compared to the shot-to-shot intensity fluctuations of scattered light. In the second scheme we used a short, delayed gate of $\tau = 250$ ns duration as depicted in Fig. 4(c). Here we set the image intensifier to high gain and the camera system was sensitive to single photons [40]. We also utilized an intensified camera as a photon number resolving detector [41] and we counted all photons with a quantum efficiency of 20% in the region of readout scattering. Representative images: single shots and averaged intensities obtained typically in those regimes are depicted in Fig. 5. Note that in Fig. 5(a) the number and localization of speckles are random so they average to the smooth intensity profile as shown in Fig. 5(b). Both measurement regimes are phase insensitive although spatially resolved, homodyne-type detection was also reported [37] and then it could be used to directly measure phase noise and squeezing properties of the generated light.

4. Results

4.1. Temporal evolution of readout intensity

At first we measured the temporal evolution of the mean number of photons emitted during readout stage. For this purpose we counted the scattered photons using an intensified camera with a gate duration of $\tau = 250$ ns. We collected all photons in the specified circular camera region around the point corresponding to the center of the read beam i.e. wave vector k_R . Thus,

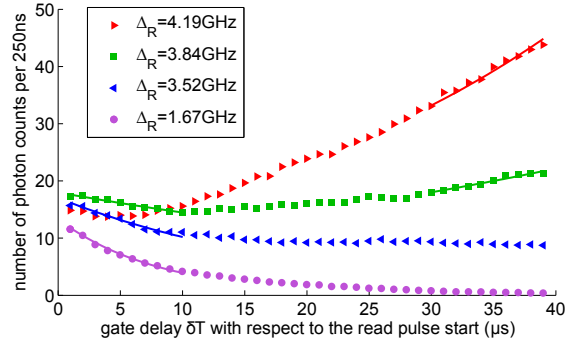


Fig. 6. Average number of photon counts detected at a large solid angle around read beam per a gate duration of 250 ns for different readout laser detunings Δ_R from ^{87}Rb $F=2 \rightarrow F'=2$ resonance. The curves represent exponential fits to the first and last data points. The size of errorbars is comparable with marker size.

we measured the anti-Stokes and the Stokes scattering together, both their spontaneous and stimulated parts. In Fig. 6 we present the results of measurement for mean number of photons versus gate delay with exponential fits. Each data point was obtained by averaging 2000 frames in the area of angular diameter 0.5 mrad and the time separation between the data points was 1 μs . The sequence was repeated for different detunings Δ_R of the read beam from $F=2 \rightarrow F'=2$ resonance.

The results plotted in Fig. 6 vividly depict a transition from decay to growth of the readout scattered light intensity. For a small detuning $\Delta_R = 1.67$ GHz the read beam is close to the $F=2 \rightarrow F'=2$ resonance and we expected the anti-Stokes coupling to dominate. Indeed, we observed an exponential decay as predicted. At the opposite extreme $\Delta_R = 4.19$ GHz, in turn, the read beam is much closer to the $F=1 \rightarrow F'=1$ transition and here it was the Stokes field that we expected to dominate. Again, the total number of scattered photons increases as expected, compare Fig. 2(c). Nonetheless, in the experiment the growth starts after the first 4 μs of the evolution during which the number of scattered photons slightly decreases. In the intermediate cases we observed initial decay followed by growth. These cases might be associated with the case presented in Fig. 2(b), where stimulated field contributions decay while the spontaneous contributions rise. Moreover, in the observed evolution the spin-wave decoherence certainly plays an important role, which, however, is not accounted for by our simplified model.

In Fig. 7 we plot decay and growth coefficients as functions of detuning Δ_R of the read beam from $F=2 \rightarrow F'=2$ resonance. The coefficients were calculated by fitting exponential decay or growth to the first or the last 10 μs , as depicted in Fig. 6. Fitting entire 40 μs with a single exponential fails because the significant influence of decoherence and multimode character of scattering on this time scale is not captured by our simple theoretical model. The dependence of the growth and decay coefficients on the detuning Δ_R agree qualitatively with predictions of the theoretical model as they rise along with Δ_R . However, there is a discontinuity between the growth and decay coefficients at $\Delta_R = 3.8$ GHz that may be attributed to spin-wave decoherence influence.

4.2. Spatial resolving of anti-Stokes and Stokes scattering

The analysis of intensity correlations between light scattered in various directions provides valuable insight into the four-wave mixing at the readout. To set the stage we shall first recall the relations between scattered photons directions. The scattering generated during the write pulse is emitted around the write beam and falls upon a circular region of angular diameter

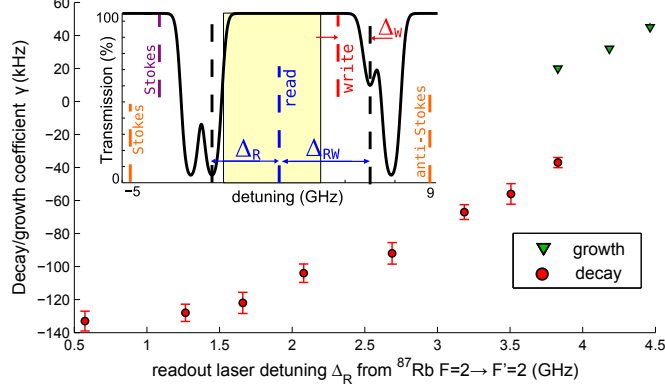


Fig. 7. Exponential decay and growth coefficients for scattered light found by fitting data as in Fig. 6 versus read laser detuning Δ_R . For triangle points the size of errorbars are smaller than the marker size. Inset: ^{87}Rb D1 line absorption spectrum with read and write laser frequencies marked.

0.5 mrad in the upper part of the camera. Similarly, the readout light illuminates the lower part of the camera of angular diameter 0.5 mrad placed in the far field. Both regions are contained in a small central part of the camera sensor. The angle between the write and read beams equal to $\theta = 2$ mrad inside the ^{87}Rb cell is precisely the distance between the centers of both circular regions on the camera. Due to phase matching illustrated in the Fig. 1(c) the scattered fields coupled to the same spin-wave with a wave vector \mathbf{K}_b propagate in different directions. They are detected in the far field on three different pixels of the camera.

For a \mathbf{K}_b oriented rightward a pixel located left of the center in the write region gathers Stokes-coupled light of an intensity proportional to the number of photons n_{WS} . Another pair of pixels, right and left of the center in the read region, gathers anti-Stokes and Stokes coupled light of intensities proportional to n_{RA} and n_{RS} respectively. Note that the latter pair of pixels also gathers light coupled to the spin-wave with an opposite wave vector $-\mathbf{K}_b$, and their role is reversed. That is, the left and the right pixels gather anti-Stokes and Stokes scattering respectively. These contributions add extra noise when correlated with Stokes scattering n_{WS} generated in the write-in process.

In order to perform correlation measurements the camera intensifier was operated in linear regime and long gate pulses were used. We detected the light scattered during both the write-in and the readout processes. In each iteration of the experiment we registered entire, randomly varying camera images. The signal I_i at the i -th pixel of the camera was proportional to the intensity of the incoming light. We calculated the correlation coefficient between intensities of light registered by any two pixels, i -th and j -th, of the camera:

$$C_{ij} = \text{corr}(I_i, I_j) = \frac{\langle I_i I_j \rangle - \langle I_i \rangle \langle I_j \rangle}{\sqrt{\langle (\Delta I_i)^2 \rangle \langle (\Delta I_j)^2 \rangle}}. \quad (5)$$

In Fig. 8(a) we present the maps of correlation coefficients C_{ij} as in Eq. (5) between one pixel marked by a cross referred as $i = WS$ and all other pixels j in the image. The pixel $i = WS$ corresponds to the emission of Stokes field coupled to the spin-wave with the wave vector $|\mathbf{K}_b| = 45.8 \text{ cm}^{-1}$. This value was set, so as to spatially resolve anti-Stokes and Stokes correlation regions. Each correlation map was calculated basing on 10^5 single-shot images. We limited our calculations to the circles marked in the maps. They correspond to the regions where the scattering was registered, centered around the directions of the write and read beams. In the

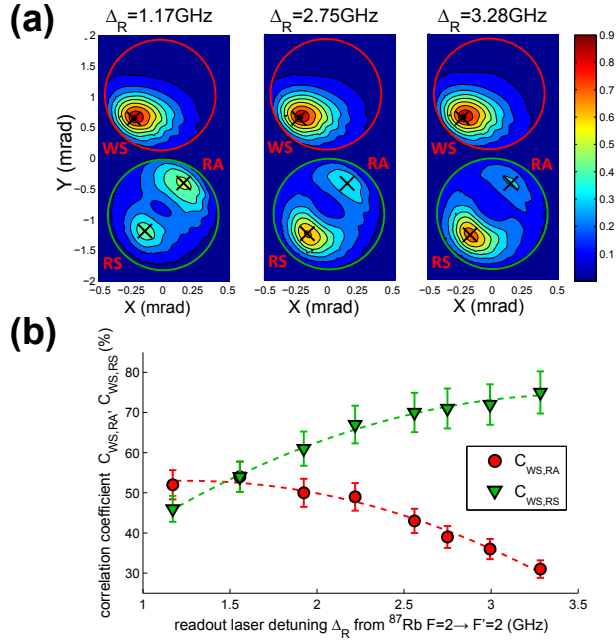


Fig. 8. (a) Spatial correlation maps for different read laser detunings from ^{87}Rb $F=2 \rightarrow F'=2$ resonance. Red and green circles mark the respective areas where photons scattered at the write and read stages fell. (b) Correlation coefficients at the peaks corresponding to anti-Stokes $C_{WS,RA}$ and Stokes $C_{WS,RS}$ versus detuning Δ_R with (quadratic) trend.

upper red circles we registered the Stokes scattering emitted in the write-in process whereas in the bottom green circles light from readout was observed.

In each map in Fig. 8(a) three spots appear. The maxima of the spots marked by the crosses on pixels $i = WS, RA, RS$ correspond to the emission of scattered fields coupled to the same spin-wave with the wave vector \mathbf{K}_b and their positions agree with the phase matching conditions illustrated in Fig. 1(c).

As we discussed in conclusion of Sec. 2, the correlation between the write scattered light and two other fields scattered at the readout stage is mediated by the spin-wave, which carries random number of excitations n_b in each iteration of the experiment. This number is proportional to the signal on the write pixel I_{WS} and contributes to the signals I_{RA} and I_{RS} . The signals on pixels far away are correlated to the excitations of other spin-waves, which vary independently. We verified that correlation maps displayed characteristic three-spot pattern for arbitrarily chosen reference points except when two spots in the readout merge. This guarantees that, indeed, we resolve the Stokes and anti-Stokes scattering in the readout. Correlation measurements are a practical alternative to spectral filtering in other experiments with quantum memories [37,42].

Now we can proceed to examine how the anti-Stokes and Stokes scattering contributions change with the read laser detuning Δ_R . In Fig. 8(a) we depicted three correlation maps for different read laser detunings Δ_R . Transition from the anti-Stokes to Stokes scattering domination can be achieved by adjusting of the detuning, here from $\Delta_R = 1.17$ GHz to $\Delta_R = 3.28$ GHz. To quantify the effect, we calculated the correlation between the Stokes scattering in write-in and the anti-Stokes scattering — $C_{WS,RA}$ or the Stokes scattering in readout — $C_{WS,RS}$. The values of $C_{WS,RA}$, $C_{WS,RS}$ were taken as the marked maxima of the respective anti-Stokes/Stokes regions for various detunings. Fig. 8(b) summarizes the results and illustrates the transition.

4.3. Effective gains of anti-Stokes and Stokes readout

The measured correlation values together with mean intensities and their variances can be used to extract information about time integrated readout gains for the anti-Stokes \bar{G}_{RA} and Stokes \bar{G}_{RS} separately. This is accomplished by tracing the origins of signal observed at respective pixels.

The signal I_{WS} registered at pixel $i = WS$ was calibrated to the number of photons. It consists of the part proportional to the number of photons n_{WS} generated during the write-in to the spin-wave of the wave vector \mathbf{K}_b and the camera system read noise f_{WS} :

$$I_{WS} = t_{WS}n_{WS} + f_{WS}, \quad (6)$$

where t_{WS} is the transmission of the write-in Stokes photons through the filter system. The read noise f_{WS} is random and its variance depends only on the intensity on the pixel $\langle(\Delta f_i)^2\rangle \sim I_i^2$. We made the calibration of the noise prior to the measurements, which allowed us to exactly determine the variance of the read noise at each pixel.

The signal in the readout at pixel $i = RA$ can be decomposed into the following contributions:

$$I_{RA} = t_{RA}n_{RA} + t_{RS}n'_{RS} + f_{RA}, \quad (7)$$

where n_{RA} is the number of photons generated in the anti-Stokes readout from the spin wave of the wave vector \mathbf{K}_b and n'_{RS} is the number of photons generated in the Stokes readout from the other spin wave with the opposite wave vector $-\mathbf{K}_b$, illuminating the same pixel. t_{RA} and t_{RS} are respectively the transmissions of the anti-Stokes and the Stokes photons and f_{RA} is the camera system read noise at the pixel $i = RA$.

We can write an analogous formula for the components of the signal registered at the pixel $i = RS$:

$$I_{RS} = t_{RS}n_{RS} + t_{RA}n'_{RA} + f_{RS}. \quad (8)$$

In the actual experiment the number of created spin-wave excitations n_b is smaller than the number of scattered photons n_{WS} due to decoherence at the write-in stage $n_b = \eta_W n_{WS}$. That factor η_W is write-in efficiency. In turn, the decoherence at the readout stage leads to a limited efficiency η_R during this process. We include those efficiencies in the formula Eq. (4), which yields the phenomenological formulas for the number of retrieved photons:

$$n_{RA} = \eta_W \eta_R \bar{G}_{RA} n_{WS} + \check{S}_{RA}, \quad (9)$$

$$n_{RS} = \eta_W \eta_R \bar{G}_{RS} n_{WS} + \check{S}_{RS}, \quad (10)$$

where \bar{G}_{RA} and \bar{G}_{RS} are the time integrated gains and \check{S}_{RA} and \check{S}_{RS} is the spontaneous emission generated at the readout introduced in the theoretical model. The factors $\eta_W \eta_R \bar{G}_{RA}$ and $\eta_W \eta_R \bar{G}_{RS}$ are the effective gains of the anti-Stokes and the Stokes readouts in the experiment.

Eqs. (7)-(10) and simple observations that $\text{corr}(n_{WS}, \eta_W \eta_R \bar{G}_{RA} n_{WS}) = 1$ and $\text{corr}(n_{WS}, \check{S}_i) = \text{corr}(n_{WS}, n'_i) = \text{corr}(n_{WS}, f_i) = 0$ allow us to calculate the effective gains from the measured quantities:

$$\eta_W \eta_R \bar{G}_{RA} = \frac{t_{WS}}{t_{RA}} \frac{C_{WS,RA} \sqrt{\langle(\Delta I_{WS})^2\rangle \langle(\Delta I_{RA})^2\rangle}}{\langle(\Delta I_{WS})^2\rangle - \langle(\Delta f_{WS})^2\rangle}, \quad (11)$$

$$\eta_W \eta_R \bar{G}_{RS} = \frac{t_{WS}}{t_{RS}} \frac{C_{WS,RS} \sqrt{\langle(\Delta I_{WS})^2\rangle \langle(\Delta I_{RS})^2\rangle}}{\langle(\Delta I_{WS})^2\rangle - \langle(\Delta f_{WS})^2\rangle}. \quad (12)$$

The above formulas can be verified by evaluating the numerators of the right hand sides.

In Fig. 9 we present the results of the effective gains of the anti-Stokes scattering $\eta_W \eta_R \bar{G}_{RA}$ and the Stokes scattering $\eta_W \eta_R \bar{G}_{RS}$ for different read laser detunings Δ_R . The efficiency due to

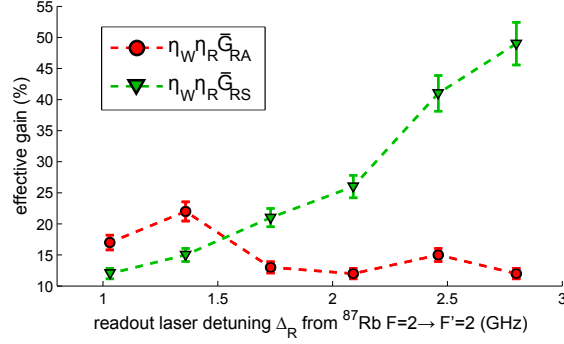


Fig. 9. The effective gains of the anti-Stokes scattering $\eta_W \eta_R \bar{G}_{RA}$ and the Stokes scattering $\eta_W \eta_R \bar{G}_{RS}$. For the smallest detuning Δ_R absorption in rubidium cell starts to contribute.

decoherence in the write-in η_W is fixed. The efficiency of the readout η_R is mostly determined by the decoherence during this process, thus it also weakly depends on the detuning Δ_R . Thus we expect that the experimentally determined effective gains vary mostly due to the change of the time integrated gains \bar{G}_i and can be compared with the theoretical predictions.

Our results show that in our configuration the Stokes scattering during readout is an important contribution to the scattered light. The highest observed efficiency of the anti-Stokes retrieval was $\eta_W \eta_R \bar{G}_{RA} = 22\%$ for $\Delta_R = 1.37$ GHz whereas the efficiency of the Stokes scattering $\eta_W \eta_R \bar{G}_{RS}$ grew with Δ_R . Note that the observed dependence of the anti-Stokes and Stokes contributions on Δ_R agrees qualitatively with our simple theoretical model for the integrated gains \bar{G}_i presented in Fig. 2(d). Note that for large detunings the anti-Stokes scattering would decay if there was no Stokes contribution. We suspect that the efficiencies values $\eta_W \eta_R \bar{G}_{RA} > 10\%$ for the anti-Stokes for $\Delta_R > 2$ GHz originated from the enhancement due to the full four-wave mixing process. The switch from domination of anti-Stokes to Stokes scattering occurs at $\Delta_R \simeq 1.5$ GHz.

In our setup we were able to manipulate the gate duration and thus check how the values of the effective gains depend on the time of interaction. We measured the effective gains for two different gate durations covering 10 μs write pulse and a part of 40 μs read pulse selected by a gate duration $\tau = 25$ μs or $\tau = 50$ μs , as we depicted in Fig. 4(b).

We measured the effective gains for two different detunings Δ_R and for the two values of the gate duration τ . We checked that the anti-Stokes effective gain $\eta_W \eta_R \bar{G}_{RA} = 12\%$ remained independent of the interaction time which indicates that light that has been correlated with the stored spin-waves is always retrieved in the beginning stage of the readout. On the other hand, the efficiency of the Stokes scattering varies, as we summarized in Table 1. As we can see, longer interaction time increases the effective gain $\eta_W \eta_R \bar{G}_{RS}$ and in particular we can obtain more correlated light than we did at the write-in stage $\eta_W \eta_R \bar{G}_{RS} > 100\%$. This corresponds to the case where the integrated gain \bar{G}_{RS} significantly exceeded unity and overcompensated

Table 1. The effective gains of the Stokes scattering $\eta_W \eta_R \bar{G}_{RS}$ for different gate durations.

Δ_R	$\eta_W \eta_R \bar{G}_{RS}$	
	$\tau = 25$ μs	$\tau = 50$ μs
2.0GHz	18%	31%
3.8GHz	93%	122%

for the losses, albeit bringing a large amount of accompanying noise \bar{S}_{RS} . Such a high gain of the obtained signal can find an application in various operations with quantum memories. For instance the dominant Stokes scattering process can be utilized for testing if the memory is empty. No photons retrieved from the memory at the readout may suggest that memory was initially empty with a certain probability. This probability is much higher for amplified readout with Stokes interaction dominant as opposed to conventional pure anti-Stokes readout process of limited efficiency.

5. Conclusions

In conclusion, we have presented an experimental demonstration of manipulation of the Hamiltonian in the readout from Raman-type atomic memory. We measured the temporal evolution of the readout light and the spatial correlations between the Raman scattering in the write-in and the readout. Our measurements confirm the adjustability of coupling parameters corresponding to the anti-Stokes and Stokes scattering. The results match our simple theoretical model of a full four-wave mixing process. We resolved the anti-Stokes and the Stokes scattering contributions to the readout thanks to the phase matching in the atomic vapor which dictated directional correlations with the Stokes photons during write-in.

Our results provide a very simple framework for interpretation of extra noise in experiments on storing light in atomic vapor. When anti-Stokes scattering is used to map the spin-wave states onto the states of light, the accompanying Stokes scattering creates unwanted random photons and atomic excitations. Our results show that, though inevitable, this contribution can be estimated by our model and perhaps suppressed by adjusting the coupling light frequency to the other side of the atomic resonance. There is also an optimal duration for the anti-Stokes interaction. Beyond the optimum, the spontaneous noise contribution increases. It may be favorable to switch to noncollinear configuration where control and quantum fields enter the atomic medium at a small angle. Then the Stokes scattering photons will become directionally distinguishable from the anti-Stokes, which may lower the noise in some experiments.

The design of the Hamiltonian we demonstrated can be implemented in many types of quantum memories at little or no extra cost. The amplification of readout signal by Stokes scattering may be very useful in some applications especially if extra noise is not crucial. This is the case when we use detectors of small quantum efficiency or we are focused on other properties of retrieved light e.g. in retrieval of stored images [23, 43]. For instance the amplification in the readout can be utilized as a robust single-shot projective test to see whether the atomic memory is in the ground (empty) state. A complete absence of Stokes signal on an inefficient detector is a relatively rare occurrence if the extra Stokes gain overcompensates for the losses at the detection stage. Notably then, complete absence of signal ensures us that the memory was in the ground state.

Our results can be useful for suppressing unconditional noise floor in readout of Raman-type quantum memories at the single photon level [13, 25, 44]. We provide evidence for a possibility of engineering a wide range of atom-light interfaces which can be described theoretically as simultaneous readout and parametric amplification e.g. quantum non-demolition interaction while coupling coefficients are equal. The facility to continuously tune the Hamiltonian coefficients sets the scene for developing new quantum protocols in room-temperature atomic memories.

Acknowledgments

We acknowledge J. Nunn for the insightful discussion and C. Radzewicz and K. Banaszek for generous support. The project was financed by the National Science Centre projects no. DEC-2011/03/D/ST2/01941 and DEC-2013/09/N/ST2/02229.